Spark plasma sintering of alumina: Study of parameters, formal sintering analysis and hypotheses on the mechanism(s) involved in densification and grain growth

Julien Gurt Santanach, Alicia Weibel, Claude Estournès, Q. Yang, Christophe Laurent, Alain Peigney

▶ **To cite this version:**

Julien Gurt Santanach, Alicia Weibel, Claude Estournès, Q. Yang, Christophe Laurent, et al.. Spark plasma sintering of alumina: Study of parameters, formal sintering analysis and hypotheses on the mechanism(s) involved in densification and grain growth. Acta Materialia, 2011, 59 (4), pp.1400-1408. 10.1016/j.actamat.2010.11.002 . hal-03544268

HAL Id: hal-03544268
https://hal.science/hal-03544268

Submitted on 26 Jan 2022

HAL is a multi-disciplinary open access archive for the deposit and dissemination of scientific research documents, whether they are published or not. The documents may come from teaching and research institutions in France or abroad, or from public or private research centers.

L'archive ouverte pluridisciplinaire **HAL**, est destinée au dépôt et à la diffusion de documents scientifiques de niveau recherche, publiés ou non, émanant des établissements d'enseignement et de recherche français ou étrangers, des laboratoires publics ou privés.

Open Archive TOULOUSE Archive Ouverte (OATAO)
OATAO is an open access repository that collects the work of Toulouse researchers and makes it freely available over the web where possible.

This is an author-deposited version published in : http://oatao.univ-toulouse.fr/
Eprints ID : 4675

To link to this article : DOI :10.1016/j.actamat.2010.11.002
URL : http://dx.doi.org/10.1016/j.actamat.2010.11.002

To cite this version : Gurt Santanach, J. and Weibel, Alicia and Estournès, Claude and Yang, Q. and Laurent, Christophe and Peigney, Alain (2011) *Spark plasma sintering of alumina: Study of parameters, formal sintering analysis and hypotheses on the mechanism(s) involved in densification and grain growth.* Acta Materialia, vol. 59 (n° 4). pp. 1400-1408. ISSN 1359-6454

Any correspondance concerning this service should be sent to the repository administrator: staff-oatao@inp-toulouse.fr.

Spark plasma sintering of alumina: Study of parameters, formal sintering analysis and hypotheses on the mechanism(s) involved in densification and grain growth

J. Gurt Santanach, A. Weibel, C. Estournès, Q. Yang, Ch. Laurent, A. Peigney *

Université de Toulouse, Institut Carnot CIRIMAT, UPS CNRS, Université Paul-Sabatier, 118 route de Narbonne, 31062 Toulouse cedex 9, France

Abstract

The spark plasma sintering (SPS) of an undoped commercial α-Al_2O_3 powder (0.14 μm) was investigated. The SPS parameters such as the dwell temperature, applied external pressure, temperature of pressure application, dwell time and pulse pattern were varied. A sintering path (relative density vs. grain size) showing two regimes has been brought to the fore: densification without grain growth occurring at the lower temperatures and grain growth without much further densification taking place at the higher temperatures, with a threshold between 1100 and 1200 °C. In addition, a formal sintering analysis was performed in order to identify the mechanism(s) involved in densification and grain growth.

Keywords: Sintering; Spark plasma sintering; Ceramics; Crystalline oxides; Alumina

1. Introduction

Spark plasma sintering [1] (SPS) is an advanced technique with a high potential for the processing of materials. SPS closely resembles hot-pressing (HP), but differs from the latter in the heating source. For SPS, a pulsed direct current is applied through the die and thus acts as the heating source by the Joule effect. From several review papers [2–4], it is observed that the aim of most SPS studies is to minimize grain growth in order to prepare dense nanostructured materials. In particular, SPS was used for the densification of Al_2O_3 specimens [5–13], including transparent samples [14–17]. Stable α-Al_2O_3 (corundum) was found to show better sintering behaviour compared with the transition γ-Al_2O_3 [5–7]. Nevertheless, specimens densified to 99.9% with an average grain size of 300 nm were prepared (1400 °C, 100 MPa, no holding time) using γ-Al_2O_3 powder 50 nm in size [8]. Submicrometre-sized α-Al_2O_3 particles were successfully sintered to dense specimens, but at conventional sintering temperatures (i.e., >1650 °C) [10]. Wang et al. [9] showed that the increase in the powder particle size into the micrometre range significantly decreases the powder sinterability. Shen et al. [12] reported a systematic study of the effect of various SPS parameters (temperature, holding time, heating rate, pressure and pulse sequence) on the densification and grain growth of a pure and MgO-doped α-Al_2O_3 powder (0.4 μm in size). An α-Al_2O_3 specimen 99.2% dense, with 600 nm average grain size, was prepared at a much lower temperature (1150 °C), within a much shorter time (minutes) than in more conventional sintering processes, but with an applied pressure of 200 MPa. These authors [12] reported that the SPS process enhances both densification and grain growth. It was further suggested that densification is enhanced in the initial part of the sintering cycle by a local spark-discharge process in the vicinity of contacting particles. Other authors [18–21] also proposed that an accumulation of electric charge on the particles surface could initiate a spark by a surface discharge and could allow plasma formation between the grains, which could explain

* Corresponding author. Tel.: +33 5 61 55 61 75; fax: +33 5 61 55 61 63.
E-mail address: peigney@chimie.ups-tlse.fr (A. Peigney).

doi:10.1016/j.actamat.2010.11.002

the efficiency of SPS (hence the name of the technique). In the case of yttrium aluminium garnet (YAG) powders, it was claimed [21–23] that such a plasma is expected to induce local surface temperatures as high as the melting temperature of the YAG particles, resulting in the formation of a viscous or even liquid layer at the particle surfaces, leading to enhanced densification and grain growth via grain sliding, rotation and grain-boundary migration within the nanometric grains, hence to the loss of the nanocrystalline character. However, some authors claim that their results advocate the absence of plasma [24]. For $MoSi_2$, Anselmi-Tamburini et al. [25] proposed that the electrical current drives densification and has an effect on grain growth by an electromigration effect. Shen et al. [12] also reported that both grain-boundary diffusion and grain-boundary migration are enhanced by the electrical field originating from the pulsed direct current. Salamon and Shen [26] investigated pressureless-SPS on pre-compacted alumina powders and obtained samples with a relative density of only 95% and high grain growth. They proposed that dynamic isotropic heating allows tremendous grain growth of α-Al_2O_3, when starting from fine powders, which takes place most probably via direct particle sliding and rotation rather than the usual epitaxial growth. Bernard-Granger and Guizard [27] reported a formal sintering analysis of SPS of a (CaO, TiO_2)-co-doped α-Al_2O_3 powder and proposed that grain-boundary sliding, accommodated by oxygen grain-boundary diffusion is controlling densification during heating and at the beginning of the dwell in the 850–1200 °C temperature range. These authors mention that they are not able to exclude a basic difference between SPS and HP and that SPS experiments on pure (i.e., undoped) Al_2O_3 are required in order to get a better understanding.

The aims of this study are thus, first, to study the influence of several SPS parameters (dwell temperature, applied external pressure, temperature of pressure application, dwell time and pulse pattern) on the densification and grain growth of a pure submicrometre-sized α-Al_2O_3 powder and secondly to perform a formal sintering analysis, in order to help formulate a hypotheses concerning the mechanism(s) controlling densification and grain growth.

2. Experimental procedure

A commercial α-alumina powder (99.99%, reference TM-DAR, Taimei Chemicals Co. Ltd.) was selected for the study. The BET (Micromeritics, Flowsorb II 2300) specific surface area was equal to 12.4 $m^2\,g^{-1}$. Field-emission-gun scanning electron microscopy (FEG-SEM; JEOL JSM 6700F operated at 5 kV) images of a powder sample metallized with Pt are shown in Fig. 1. The powder constituted from aggregates, ~5 μm in size (Fig. 1a), which are made up of particles averaging 0.14 μm in size (Fig. 1b).

The powder was sintered by SPS (Dr. Sinter 2080, SPS Syntex Inc., Japan) into an 8-mm-inner-diameter graphite die. A graphitic sheet was placed between the punches and the powder, and between the die and the powder for easy removal. Sintering was performed in vacuum (residual cell pressure <10 Pa). An optical pyrometer, focused on a small hole at the surface of the die, was used to measure and adjust the temperature. Several series of experiments were performed. For all sintering, heating rates of 150 °C min^{-1} and 100 °C min^{-1} were used from room temperature to 600 °C and from 600 °C to the desired temperature, respectively. The cooling rate was fixed to 100 °C min^{-1} for all samples. The uniaxial pressure was released during cooling for all samples. The heating was performed with a pulsed current controlled by a pulse pattern *X*–*Y*. *X* is the number of pulses (each 3.3 ms long) of current ("on-time"), and *Y* is the number of periods (each 3.3 ms long) when there is no current ("off-time"). The following parameters were studied: dwell temperature (600, 900, 1000, 1050, 1100, 1200, 1300 and 1500 °C, specimens A), applied pressure (10, 30, 50 and 100 MPa, specimens B), temperature of pressure application (600, 900 and 1200 °C, specimens C), dwell time (0, 1, 3, 5, 15 and 60 min, specimens D) and pulse pattern (3–2, 12–2, 24–2, 70–2 and 98–2, specimens E). Selected conditions were chosen for a formal sintering analysis (specimens F).

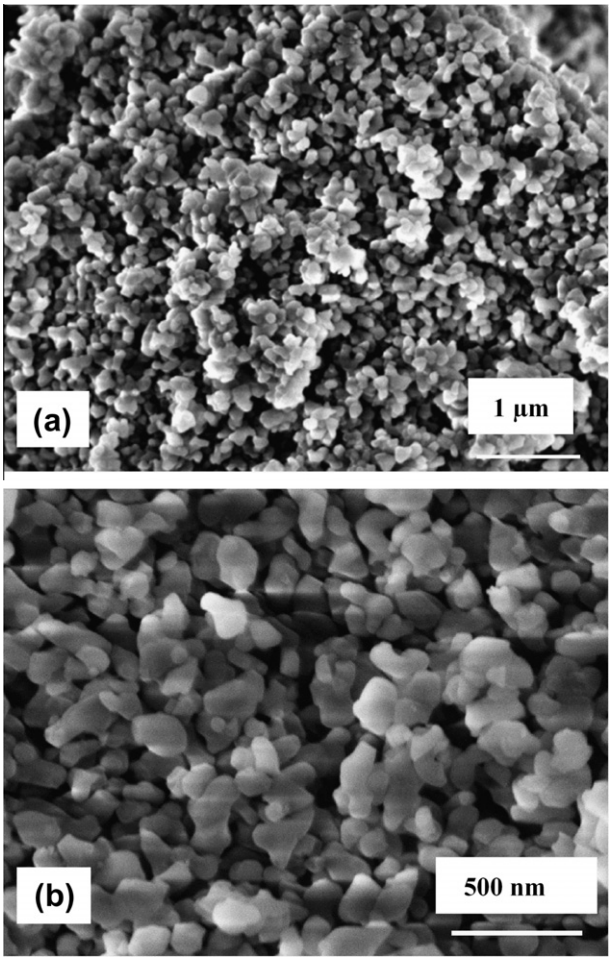

Fig. 1. FEG-SEM images of the α-alumina powder at (a) low and (b) high magnifications.

The sintered specimens were in the form of pellets 8 mm in diameter and close to 2 mm thick. The density was

determined after removal of the graphitic surface sheet by light polishing. It was first estimated from the weight and dimensions and also measured by the Archimedes method only for samples presenting a low porosity (relative density >92%). The sintered samples were metallized with Pt and observed by FEG-SEM. The average grain size was estimated on images of the fracture surfaces from the measurement of several hundred grains. A selected specimen was observed by transmission electron microscopy (TEM; JEOL JEM 2100F operated at 200 kV). The corresponding sample was prepared using a grinding, dimpling and ion-milling routine.

3. Results and discussion

3.1. Influence of the dwell temperature (specimens A)

The influence of the dwell temperature (600, 900, 1000, 1050, 1100, 1200, 1300 and 1500 °C) was studied while maintaining constant the other experimental conditions (in particular, the pressure was applied at 600 °C) (Table 1). The relative densities (D) and grain sizes (G) are reported in Table 1 and Fig. 2a. Specimen A1 was sintered at only 600 °C, and the corresponding relative density is equal to 54.6%. For A2 (900 °C) and A3 (1000 °C), there is only a moderate increase (58.4% and 62.7%, respectively). By contrast, D increases sharply for A4 (1050 °C, 80.5%) and A5 (1100 °C, 94.5%) and then reaches a plateau (98.5%, 99.2% and 99.2% for A6, A7 and A8, respectively). The grain size is constant (0.2 μm) for A1–A5 and increases progressively on increase in the dwell temperature, reaching 7.6 μm for A8 (1500 °C). Typical FEG-SEM images are shown in Fig. 3. The sintering trajectory, represented by a plot of D vs. G, is shown in Fig. 2b. The two steps of the sintering process are clearly identified: densification without grain growth at the lower temperatures and grain growth without much further densification at the higher temperatures. The threshold is between 1100 and 1200 °C, less than 100 °C higher than for a co-doped powder [27].

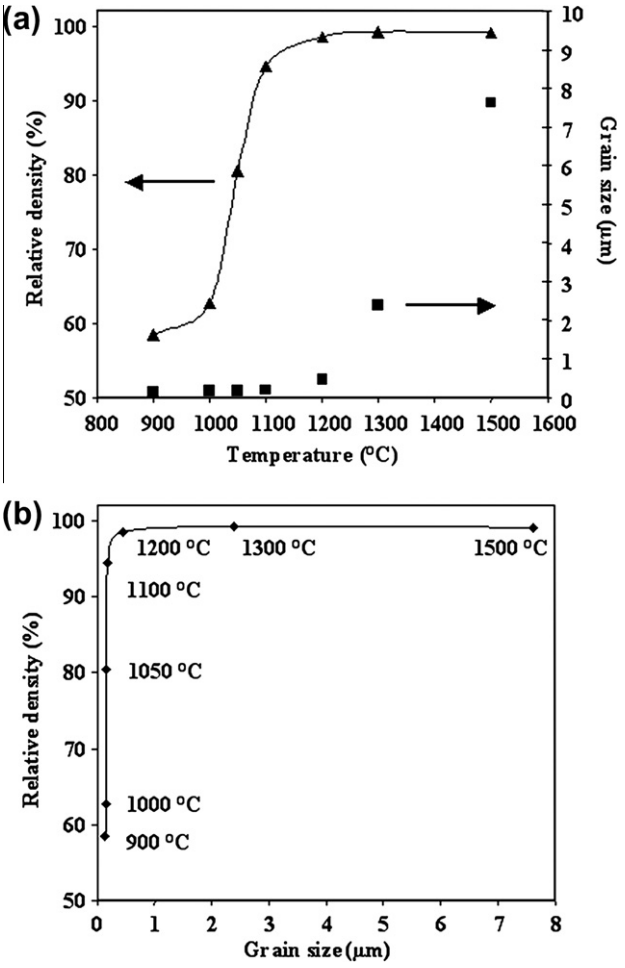

Fig. 2. (a) Relative density (triangles) and grain size (squares) vs. dwell temperature; (b) sintering path (relative density vs. grain size).

3.2. Influence of applied pressure (specimens B)

The influence of the applied pressure (10, 30, 50 and 100 MPa) was studied while maintaining constant the other experimental conditions (Table 2). All four specimens show the same relative density (~99%), as expected from the results presented in Section 3.1, but G increases from 4.3 μm (B1, 10 MPa) to 7.5 μm (B4, 100 MPa) (Table 2). Thus, increasing the applied pressure favours grain growth, in agreement with Shen et al. [12], who reported that applying a higher pressure and higher temperature could favour the increase in relative density and could thus increase the grain size through grain-boundary diffusion.

Table 1
SPS parameters for the study of the influence of the dwell temperature: T, dwell temperature; t, dwell time; P, uniaxial pressure; T_P, temperature of pressure application; (X–Y), pulse pattern; D, relative density (±0.2%); G, average grain size (±0.1 μm).

Specimen	T (°C)	t (min)	P (MPa)	T_P (°C)	(X–Y)	D (%)	G (μm)
A1	600	5	100	600	12–2	54.6	0.2
A2	900					58.4	0.2
A3	1000					62.7	0.2
A4	1050					80.5	0.2
A5	1100					94.5	0.2
A6	1200					98.5	0.5
A7	1300					99.2	2.4
A8	1500					99.2	7.6

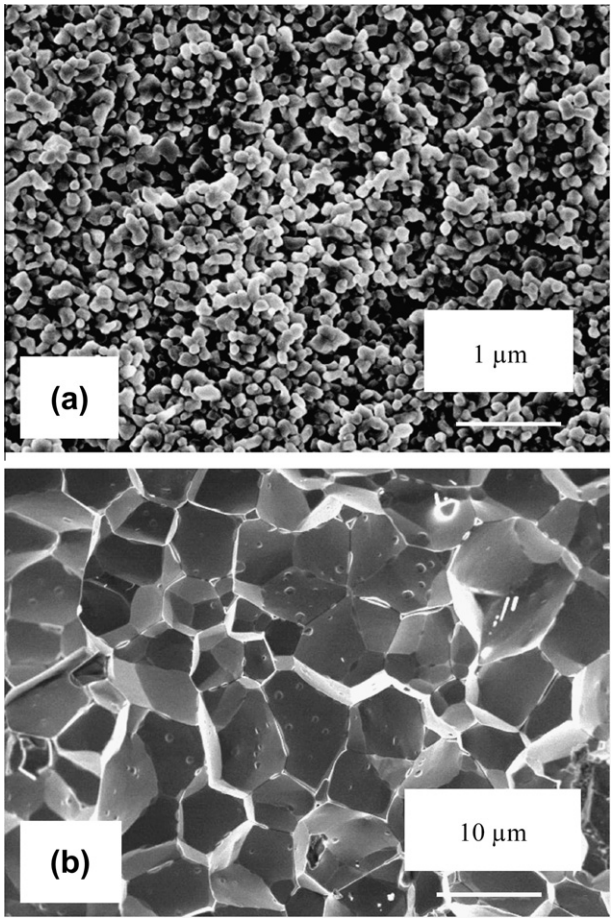

Fig. 3. FEG-SEM images of fracture surface of the (a) A3 and (b) A8 specimens.

3.3. Influence of the temperature of pressure application (specimens C)

The influence of the temperature of pressure application (600, 900 and 1200 °C) was studied, while maintaining constant the other experimental conditions (Table 3). There is no effect on grain size, but a small increase in relative density, from 98.9% for C1 to 99.7% for C3, on the increase in temperature of pressure application, which could reflect easier particle sliding or rotation when the pressure is applied at a higher temperature [23]. Interestingly, C3 was a translucent material.

3.4. Influence of the dwell time (specimens D)

The influence of the dwell time (0, 1, 3, 5, 15 and 60 min) was studied while maintaining the other experimental conditions constant (Table 4). The first group of samples (D1–D5) was sintered at 1000 °C and another group (D6–D10) was sintered at 1100 °C. The results are reported in Table 4 and Fig. 4. At 1000 °C, D regularly increases upon the increase in dwell time, from 64.4% (D1, 0 min) to 86.1% (D5, 60 min), whereas G is constant (0.2 μm). The dwell time could thus be used to control the proportion of porosity in the specimen precisely. At 1100 °C, D is always higher than for the D1–D5 specimens and again regularly increases on increase in dwell time, from 90.8% (D6, 0 min) to 99.8% (D10, 60 min). There is no increase in grain size for a dwell up to 5 min, but higher G values are observed for the longer dwell times, reaching 0.3 and 0.5 μm for D9, 15 min and D10, 60 min, respectively.

3.5. Influence of the pulse pattern (specimens E)

The influence of the pulse pattern (3–2, 12–2, 24–2, 70–2 and 98–2) was studied while maintaining constant the other experimental conditions (Table 5). In fact, only the on-time (X) was varied, and the off-time was kept constant ($Y = 2$). The reverse (keeping X constant and varying Y) was also tried and gave similar results. The first group of samples (E1–E5) was sintered at a temperature (1100 °C) in the densification regime and another group (E6–E10) was sintered at a temperature (1500 °C) in the grain-growth regime. Whatever the sintering temperature, the pulse pattern has no or little influence on the grain size and density (Table 5), in agreement with earlier results [12].

3.6. Formal sintering analysis in the densification regime

As mentioned by Bernard-Granger and Guizard [27,28], matter transport during sintering with or without an external load can be considered as analogous to that occurring in high-temperature creep [29,30], and the HP kinetic equation can be written in a simplified version [31] of the general relationship for steady-state creep strain [32]. Therefore, the HP equation (Eq. (1)) was considered:

$$\frac{1}{D}\frac{dD}{dt} = \frac{B\Phi\mu_{\text{eff}}b}{kT}\left(\frac{b}{G}\right)^{p}\left(\frac{\sigma_{\text{eff}}}{\mu_{\text{eff}}}\right)^{n} \quad (1)$$

Table 2
SPS parameters for the study of the influence of the applied pressure; symbols as in Table 1 except: G, average grain size (±0.2 μm).

Specimen	T (°C)	T (min)	P (MPa)	T_P (°C)	(X–Y)	D (%)	G (μm)
B1			10			99.1	4.3
B2	1500	3	30	600	12–2	99.2	6.7
B3			50			99.2	6.7
B4			100			99.1	7.6

Table 3
SPS parameters for the study of the influence of the temperature of pressure application; symbols as in Table 1.

Specimen	T (°C)	T (min)	P (MPa)	T_P (°C)	(X–Y)	D (%)	G (μm)
C1				600		98.9	0.5
C2	1200	3	100	900	12–2	99.5	0.5
C3				1200		99.7	0.3

Table 4
SPS parameters for the study of the influence of the dwell time: symbols as in Table 1.

Specimen	T (°C)	T (min)	P (MPa)	T_P (°C)	(X–Y)	D (%)	G (μm)
D1		0				64.4	0.2
D2		1				69.6	0.2
D3	1000	5	100	600	12–2	74.4	0.2
D4		15				79.3	0.2
D5		60				86.1	0.2
D6		0				90.8	0.2
D7		1				91	0.2
D8	1100	5	100	600	12–2	96.8	0.2
D9		15				99	0.3
D10		60				99.8	0.5

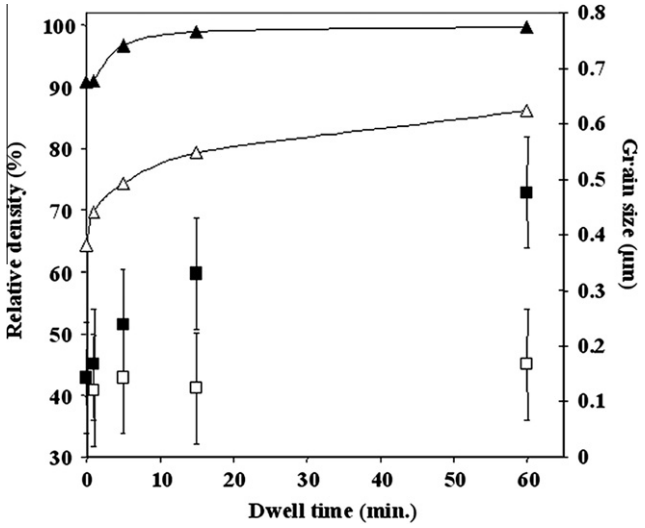

Fig. 4. Relative density (open triangles, 1000 °C; solid triangles, 1100 °C) and grain size (open squares, 1000 °C; solid squares, 1100 °C) vs. dwell time.

where D is the instantaneous relative density, B is a constant, G is the grain size, σ_{eff} is the instantaneous effective stress acting on the powder bed, μ_{eff} is the effective shear modulus of the powder bed, Φ is the diffusion coefficient, t is time, b is the Burgers vector, k is the Boltzmann constant, and p and n are the exponents for grain size and stress, respectively.

According to Helle et al. [33], σ_{eff} can be described by:

$$\sigma_{eff} = \frac{1 - D_0}{D(D - D_0)}\sigma_{mac} \tag{2}$$

where σ_{mac} is the macroscopic compaction pressure (0.025 GPa or 0.1 GPa) applied to the powder bed, and D_0 is the green density (taken as 54.6% from specimen A1; Table 1). The effective shear modulus μ_{eff} of the compacted powder bed can be described by:

$$\mu_{eff} = \frac{E_{th}(D - D_0)}{2(1 + \nu_{eff})(1 - D_0)} \tag{3}$$

Table 5
SPS parameters for the study of the influence of the pulse pattern: symbols as in Table 1, except G, average grain size (±0.1 μm for E1–E5 and ±0.5 μm for E6–E10).

Specimen	T (°C)	t (min)	P (MPa)	T_P (°C)	(X–Y)	D (%)	G (μm)
E1					3–2	88.4	0.2
E2					12–2	89.6	0.2
E3	1100	3	100	600	24–2	83.7	0.2
E4					70–2	87	0.2
E5					98–2	86	0.2
E6					3–2	98.9	9.5
E7					12–2	98.9	7.6
E8	1500	3	100	600	24–2	98.9	8.5
E9					70–2	98.8	7.2
E10					98–2	98.8	9.9

where E_{th} is Young's modulus (400 GPa), and v_{eff} is Poisson's ratio (0.25). In the temperature range 900–1000 °C corresponding to the densification regime, as opposed to the grain-growth regime, Eq. (1) can be rewritten [27,28] as:

$$\frac{1}{\mu_{eff}}\frac{1}{D}\frac{dD}{dt} = K_0\frac{e^{-\frac{Qd}{kT}}}{T}\left(\frac{\sigma_{eff}}{\mu_{eff}}\right)^n \quad (4)$$

where K_0 is a constant, and Q_d is the activation energy of the mechanism controlling densification. To determine n, Eq. (4) was transformed into its logarithmic form (Eq. (5)):

$$\ln\left[\frac{1}{\mu_{eff}}\frac{1}{D}\frac{dD}{dt}\right] = n\cdot\ln\left(\frac{\sigma_{eff}}{\mu_{eff}}\right) + K_1 \quad (5)$$

where K_1 is a constant for a fixed temperature. The dwell temperatures used for this part of the study were 900, 950 and 1000 °C in order to avoid any grain growth (specimens F1, F2 and F3, respectively). A dwell time of 15 min and a pulse pattern of 12–2 were used. The pressure (100 MPa) was applied at 600 °C. In addition, a fourth sintering (specimen F4) was performed at 1000 °C under a pressure of only 25 MPa, thus in conditions close to those usually used in HP. The evolution of the relative density during the dwell is reported in Fig. 5a. The value achieved for D is ~76% for F1, close to 80% for F2 and F3, and only 71% for F4. The stress exponent n was determined as the slope of the plot of Eq. (5) (Fig. 5b). For F4, n is equal to 2.10, which corresponds to a densification mechanism by grain-boundary sliding [34] or by interface reactions [35]. This n value was also reported by Xue and Chen [36] and Cannon et al. [37] for the HP of Al_2O_3, in experimental conditions close to the present ones. By contrast, n is much higher when a pressure of 100 MPa is used and increases with the sintering temperature ($n = 3.95$, 4.21 and 4.67 for F1, F2 and F3, respectively). According to the HP densification model, the high densification rates obtained for moderate temperatures (900–1000 °C) but under high pressure (100 MPa) could correspond to creep by dislocation climb ($n > 3$) or to plastic deformation ($n > 4.5$) [38]. Using $n = 4$ as an approximate value of the stress exponent, the activation energy of densification was evaluated as $Q_d = 644$ kJ mol^{-1}, using Eq. (4) transformed as (Fig. 6):

$$\ln\left[\frac{T}{\mu_{eff}}\left(\frac{\mu_{eff}}{\sigma_{eff}}\right)^4\frac{1}{D}\frac{dD}{dt}\right] = -\frac{Q_d}{RT} + K_2 \quad (6)$$

where K_2 is a constant. This Q_d value is over twice that determined for a co-doped powder [27], but is close to those reported by several authors for the HP of Al_2O_3 powders with different particle size. Indeed, Sato and Carry [39] found values in the range 617–653 kJ mol^{-1} (particle size ~0.3 μm), Johnson and Cuttler [40] reported values in the range 593–627 kJ mol^{-1} (particle size in the range 0.3–0.6 μm), Shiau et al. [41] found 667 kJ mol^{-1} (average particle size equal to ~0.3 μm) and Opfermann et al. [42] reported a value of 660 kJ mol^{-1} (micrometric particles). All these authors [39–42] proposed a mechanism of grain-boundary diffusion of the Al^{3+} ions. Note, however, that the Q_d value obtained is very sensitive to the value of n used for the calculation. Nevertheless, it appears that there is a discrepancy between the densification mechanism suggested by the present Q_d value (grain-boundary diffusion) and that suggested by the present n values (dislocation climb or plastic deformation). However, the latter mechanisms have been identified so far only for MgO and cubic ZrO_2, but not for alumina, and for much higher sintering temperatures (>1500 °C) and seem difficult to account for in the present case.

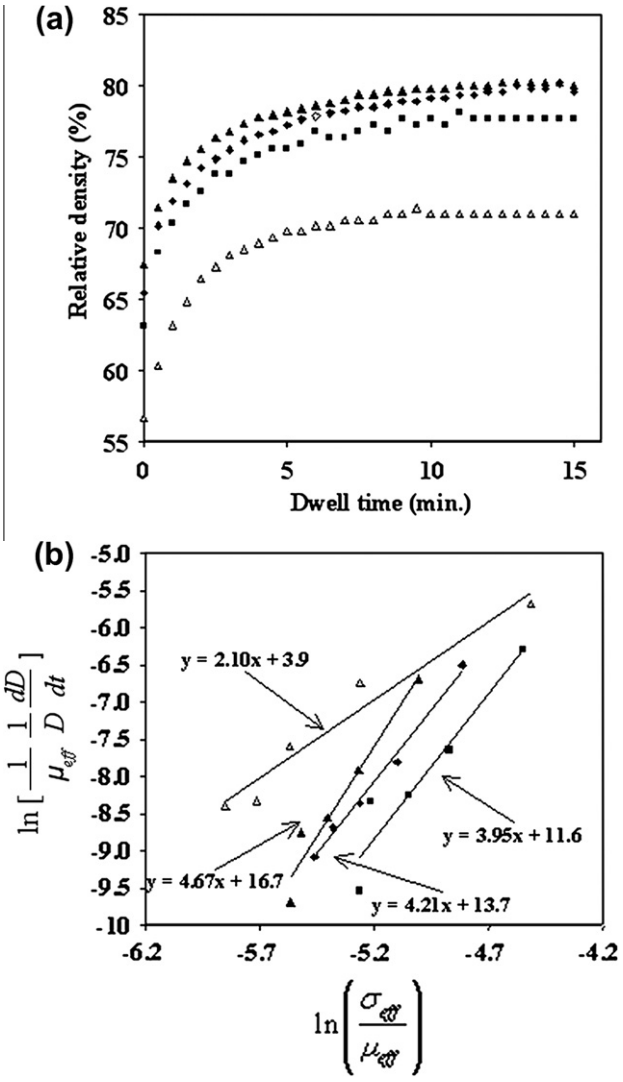

Fig. 5. (a) Evolution of the relative density during the dwell; (b) plot of Eq. (5) and determination of the slope of the interpolated lines (stress exponent n); solid squares (900 °C, 100 MPa), solid diamonds (950 °C, 100 MPa), solid triangles (1000 °C, 100 MPa), open triangles (1000 °C, 25 MPa).

Therefore, it was attempted to identify potential sources of error when using the HP model for SPS. It was first envisaged that the value of D_0 (density at 600 °C) is inappropriate because of the possibility of grain rearrangement during the heating step to the dwell temperature, which could alter the connectivity of the grains. However, no

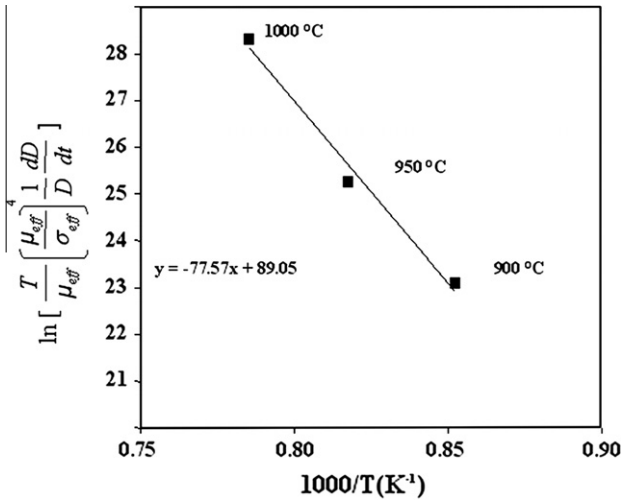

Fig. 6. Plot of Eq. (6) and determination of the slope of the interpolated line ($-Q_d/R$).

shrinkage was observed between 600 and 800 °C, which ruled out the possibility of further grain rearrangement above 600 °C, the temperature at which the maximum pressure (100 MPa) is achieved. It was also considered that the correction factor used (Eq. (2)) to calculate the effective stress σ_{eff} is inappropriate. Other correction factors were therefore used. However, the n values thus obtained were unreasonable ($n > 12$). These results lead us to rule out these possible sources of error in the application of the model.

On the one hand, assuming that the HP model remains appropriate for SPS under high pressure conditions and moderate temperature, specific mechanisms were considered. Wachtman [43] investigated the creep of Al_2O_3 and suggested the possibility of plastic deformation of submicronic grains at temperatures of the order of 1000 °C for a pressure of 100 MPa, which could be in agreement with the values of the present exponent n ($n \geqslant 4$). This could occur for a temperature as low as 900 °C because of the very low grain size (0.14 μm) of the present powder. However, a TEM observation of specimen F3 (Fig. 7) did not reveal the presence of dislocations. Thus, it is not realistic to propose that the present n values are representative of dislocation climb or plastic deformation for SPS.

On the other hand, one must also consider that the HP model is not suitable for SPS, at least for high applied pressures. Olevsky and Froyen [44] have proposed a model including thermal-diffusion which, while admittedly incomplete, is claimed to be suitable for the description of any rapid sintering technique, including SPS. It could also be considered that there is particular electrical effect during SPS. For the SPS of ceramic nanopowders under high pressure (100 MPa), it was proposed [21,23] that a thin liquid layer appears on the surface of the grains owing to discharge or plasma phenomena, leading to a grain rearrangement by rotation, and thus to very fast densification. A microscopy study will be undertaken to analyze the surface

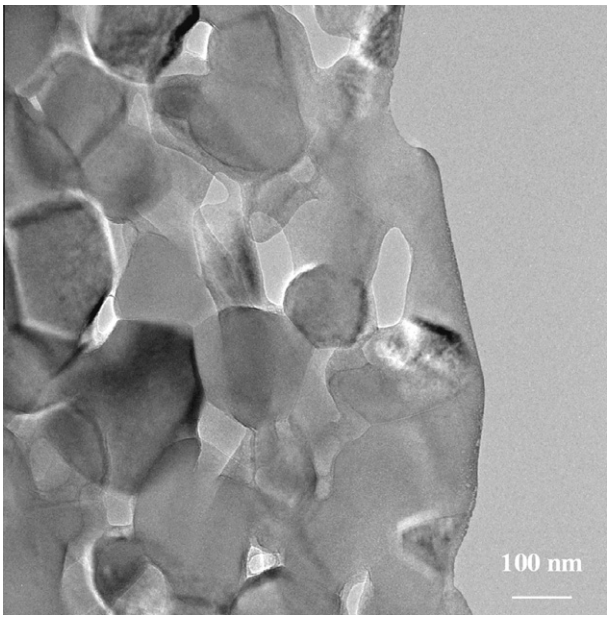

Fig. 7. TEM image of specimen F3 revealing no dislocations.

of the grains and the grain boundaries, in particular, in order to differentiate the two types of mechanism obtained for 1000 °C with either 25 or 100 MPa.

3.7. Formal sintering analysis in the grain-growth regime

The isothermal-grain-growth coefficient m was determined in order to throw some light on the grain growth mechanisms. This was done for sample D9 (1100 °C, 15 min, 100 MPa, Table 4), 1100 °C being a temperature at which grain growth is low but observable. The model for grain growth is represented by:

$$G_t^m - G_0^m = Kt \tag{7}$$

where G_t and G_0 are the grain size at time t and $t = 0$, respectively, m is the grain-growth exponent, and K is a constant [45]. For a monophased system, m can be equal to 2, 3 or 4, which corresponds to growth by grain-boundary diffusion, volume or through a liquid-phase diffusion or surface diffusion. Eq. (7) was plotted using $G_t = 0.3$ μm (Table 4) and $G_0 = 0.14$ μm for the three values of m (Fig. 8). According to the regression coefficients R^2, two m values are acceptable ($R^2 = 0.999$ for $m = 4$ and $R^2 = 0.996$ for $m = 3$). For $m = 4$, growth would occur by surface diffusion, which requires a high proportion of free surface (i.e., porosity) to be active. However, it should be noted that the relative density of the sample is higher than 80% when the isotherm is reached and is ~99% after only 15 min at the dwell temperature. This could rule out surface diffusion. For $m = 3$, growth would occur by volume diffusion or diffusion through a local liquid phase. As mentioned above, a liquid layer could be present on the surface of the grains owing to locally very high temperatures caused by discharges or by plasma [21,23]. The

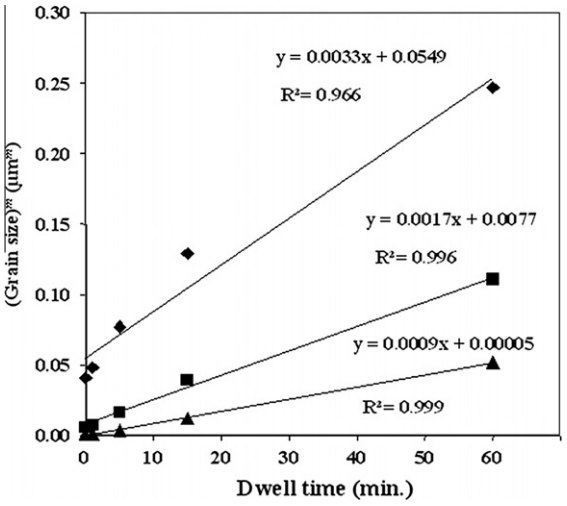

Fig. 8. Plots of Eq. (7) for different values of grain-growth exponent m (diamonds, $m = 2$; squares, $m = 3$; triangles, $m = 4$) and determination of the R^2 factor of the interpolated lines for specimen D9.

presence of a liquid phase, which remains speculative, could account for the rapid densification obtained for lower temperatures (900, 950 and 1000 °C).

4. Conclusions

The spark plasma sintering of an undoped commercial α-Al_2O_3 powder (0.14 μm) was investigated. A sintering path showing two separate regimes has been brought to light: densification without grain growth occurring at the lower temperatures and grain growth without much further densification taking place at the higher temperatures, the threshold being between 1100 and 1200 °C. In the grain-growth regime, increasing the applied pressure tends to favour grain growth, possibly through grain-boundary diffusion. Delaying the temperature of pressure application could produce a small increase in relative density, without any adverse effect on grain size, which could reflect better powder packing because of easier particle sliding or rotation at higher temperatures. Increasing the dwell time at 1000 °C (densification regime) produces a regular increase in relative density, reaching 86.1% for 60 min with a grain size of 0.2 μm. The dwell time could thus be used to control the proportion of porosity in the specimen precisely. At 1100 °C (grain-growth regime), the relative density also regularly increases upon the increase in dwell time, reaching 99.8% for 60 min with a grain size of 0.5 μm. Changing the pulse pattern while maintaining the other experimental conditions constant did not influence the relative density or the grain size. In the second part of the study, a formal sintering analysis was performed in both the densification and grain-growth regimes. In the densification regime, determination of the stress exponent using the model developed for HP suggests a densification mechanism by grain-boundary sliding or by interface reactions for a low applied pressure (25 MPa). By contrast, for a higher pressure (100 MPa), this analysis points towards dislocation climb or plastic deformation, both of which are unlikely mechanisms for α-Al_2O_3 in this temperature range, whereas the evaluated activation energy of densification (644 kJ mol^{-1}) points towards grain-boundary diffusion of the Al^{3+} ions. TEM observation of a selected specimen did not reveal the presence of dislocations, and therefore it is proposed that the HP model is not suitable for SPS, at least for high applied pressures. Particular electrical effects during SPS should probably be considered, involving mechanisms including thermal-diffusion and local softening/melting of the grain surfaces owing to very high local temperatures caused by discharges or by plasma, to account for the fast densification. In the grain-growth regime, the analysis points towards volume diffusion or diffusion through a local liquid phase. The presence of such a liquid phase, or at least softened grain surfaces remains speculative and warrants further studies.

Acknowledgements

The FEG-SEM and TEM observations were performed at TEMSCAN, the "Service Commun de Microscopie Electronique à Transmission", Université Paul-Sabatier. The SPS was performed at the Plateforme Nationale CNRS de Frittage-Flash (PNF^2, Toulouse). The authors thank Dr. C. Elissalde (ICMCB, Bordeaux) for the preparation of the sintered alumina TEM sample and Y. Parant-hoen (Société des Céramiques Techniques, Bazet) for JGS doctoral thesis grant. This work was performed under the ANR-06-NANO-049 programme.

References

[1] Tokita M. J Soc Powder Technol Jpn 1993;30:790.
[2] Shen Z, Nygren M. Key Eng Mater 2003;247:79.
[3] Munir A, Anselmi-Tamburini U, Ohyanagi M. J Mater Sci 2006;41:763.
[4] Chaim R, Levin M, Shlayer A, Estournès C. Adv Appl Ceram 2008;27:159.
[5] Risbud SH, Shan CH, Mukherjee AK, Kim MJ, Bow JS, Holl RA. J Mater Res 1995;10:237.
[6] Mishra RS, Risbud SH, Mukherjee AK. J Mater Res 1998;13:86.
[7] Mishra RS, Mukherjee AK. Mater Sci Eng 2000;A287:178.
[8] Zhao Z, Buscaglia V, Bowen P, Nygren M. Key Eng Mater 2004;264–268:2297.
[9] Wang SW, Chen LD, Hirai T. J Mater Res 2000;15:982.
[10] Gao L, Hong JS, Miyamoto H, Torre SDDL. J Eur Ceram Soc 2000;20:2149.
[11] Oh ST, Tajima KI, Ando M, Ohji T. J Am Ceram Soc 2000;83:1314.
[12] Shen Z, Johnsson M, Zhao Z, Nygren M. J Am Ceram Soc 2002;85:1921.
[13] Palmero P, Locci A, Tulliani JM, Orru R, Cao G, Montanaro L. Adv Sci Technol 2006;45:957.
[14] Kim BN, Hiraga K, Morita K, Yoshida H. Scripta Mater 2007;57:607.
[15] Aman Y, Garnier V, Djurado E. J Eur Ceram Soc 2009;29:3363.
[16] Omori M. Mater Sci Eng 2000;A287:183.
[17] Jiang DT, Hulbert DM, Anselmi-Tamburini U, Ng T, Land D, Mukherjee AK. J Am Ceram Soc 2008;91:151.
[18] Omori M. Mater Sci Eng 2000;A 287:183.

[19] Shon IJ, Munir ZA. Mater Sci Eng 1995;A202:256.
[20] Tokita M. Mater Sci Forum 1999;83:308.
[21] Chaim R. J Mater Sci 2006;41:7862.
[22] Chaim R, Marder-Jaeckel R, Shen JZ. Mater Sci Eng 2006;A429:74.
[23] Chaim R. Mater Sci Eng 2007;A443:25.
[24] Hulbert DM, Anders A, Andersson J, Lavernia EJ, Mukherjee AK. Scripta Mater 2009;60:835.
[25] Anselmi-Tamburini U, Garay JE, Munir ZA. Mater Sci Eng 2005;A407:24.
[26] Salamon D, Shen Z. Mater Sci Eng 2008;A475:105.
[27] Bernard-Granger G, Guizard C. J Mater Res 2009;24:179.
[28] Bernard-Granger G, Guizard C. Acta Mater 2007;55:3493.
[29] Brook RJ, Gilbert E, Hind D, Vieira JM. Sintering – theory and practice. Elsevier: Amsterdam; 1982. p. 585.
[30] Coble RL. J Appl Phys 1970;41:4789.
[31] Bordia RK, Raj R. J Am Ceram Soc 1988;71:302.
[32] Mukherjee AK, Bird JE, Dorn JE. Trans ASM 1969;62:155.
[33] Helle AS, Easterling KE, Ashby MF. Acta Metall 1985;33:2163.
[34] Langdon TG. Philos Mag 1970;22:689.
[35] Ashby MF. Scripta Metall 1969;3:837.
[36] Xue LA, Chen IW. J Am Ceram Soc 1990;73:3518.
[37] Cannon RM, Rhodes WH, Heuer AH. J Am Ceram Soc 1979;63:46.
[38] Vieira JM, Brook RJ. J Am Ceram Soc 1984;67:245.
[39] Sato E, Carry C. J Eur Ceram Soc 1995;15:9.
[40] Johnson DL, Cuttler IB. J Am Ceram Soc 1963;46:545.
[41] Shiau FH, Fang TT, Leu TH. Mater Chem Phys 1998;57:33.
[42] Opfermann J, Blumm J, Emmerich WD. Thermochim Acta 1998;318:213.
[43] Wachtman JB. Mechanical properties of ceramics. NY: JohnWiley; 1996. p. 302.
[44] Olevsky E, Froyen L. J Am Ceram Soc 2009;92:S122.
[45] Chaim R, Shlayer A, Estournès C. J Eur Ceram Soc 2009;29:91.